2010

Identification and Characterization of Oxalate Oxidoreductase, a Novel Thiamine Pyrophosphate-dependent 2-Oxoacid Oxidoreductase That Enables Anaerobic Growth on Oxalate

Elizabeth Pierce
University of Michigan, Ann Arbor

Donald F. Becker
University of Nebraska-Lincoln, dbecker3@unl.edu

Stephen W. Ragsdale
University of Michigan, Ann Arbor, sragsdal@umich.edu

THE JOURNAL OF BIOLOGICAL CHEMISTRY VOL. 285, NO. 52, pp. 40515–40524, December 24, 2010

Identification and Characterization of Oxalate Oxidoreductase, a Novel Thiamine Pyrophosphate-dependent 2-Oxoacid Oxidoreductase That Enables Anaerobic Growth on Oxalate*[S]

Received for publication, June 17, 2010, and in revised form, October 15, 2010 Published, JBC Papers in Press, October 18, 2010, DOI 10.1074/jbc.M110.155739

Elizabeth Pierce[‡], Donald F. Becker[§], and Stephen W. Ragsdale[‡1]

From the [‡]Department of Biological Chemistry, University of Michigan, Ann Arbor, Michigan 48109-0606 and the [§]Department of Biochemistry, University of Nebraska, Lincoln, Nebraska 68588-0664

Moorella thermoacetica **is an anaerobic acetogen, a class of bacteria that is found in the soil, the animal gastrointestinal tract, and the rumen. This organism engages the Wood-Ljungdahl pathway of anaerobic CO_2 fixation for heterotrophic or autotrophic growth. This paper describes a novel enzyme, oxalate oxidoreductase (OOR), that enables *M. thermoacetica* to grow on oxalate, which is produced in soil and is a common component of kidney stones. Exposure to oxalate leads to the induction of three proteins that are subunits of OOR, which oxidizes oxalate coupled to the production of two electrons and CO_2 or bicarbonate. Like other members of the 2-oxoacid: ferredoxin oxidoreductase family, OOR contains thiamine pyrophosphate and three $[Fe_4S_4]$ clusters. However, unlike previously characterized members of this family, OOR does not use coenzyme A as a substrate. Oxalate is oxidized with a k_{cat} of 0.09 s^{-1} and a K_m of 58 μM at pH 8. OOR also oxidizes a few other 2-oxoacids (which do not induce OOR) also without any requirement for CoA. The enzyme transfers its reducing equivalents to a broad range of electron acceptors, including ferredoxin and the nickel-dependent carbon monoxide dehydrogenase. In conjunction with the well characterized Wood-Ljungdahl pathway, OOR should be sufficient for oxalate metabolism by *M. thermoacetica*, and it constitutes a novel pathway for oxalate metabolism.**

Moorella thermoacetica is a strictly anaerobic Gram-positive acetogenic bacterium. Acetogens are commonly found in the soil, animal gastrointestinal tract, and the rumen and grow heterotrophically or autotrophically on many different electron donors. Electrons from these substrates are used to reduce CO_2 to acetate by the Wood-Ljungdahl pathway. During growth by this pathway, acetate and cell mass are the only growth products, and electron-rich growth substrates like glucose are converted stoichiometrically to acetate; therefore, *M. thermoacetica* is called a homoacetogen. *M. thermoacetica* can use other electron acceptors (*e.g.* nitrate, nitrite, thiosulfate, and dimethyl sulfoxide). Under most conditions, nitrate reduction occurs preferentially to CO_2 reduction, and nitrate has been shown to repress autotrophic growth (1, 2). However, oxalate is unique in its properties as an electron donor by *M. thermoacetica* for acetogenic growth. When both nitrate and CO_2 are provided to cells growing on oxalate, CO_2 is reduced to acetate during exponential growth phase, and nitrate is only used as the electron acceptor during stationary phase (3). Oxalate is the only substrate with which *M. thermoacetica* has been shown to reduce CO_2 instead of nitrate when both are present.

Oxalate ($C_2O_4^{2-}$) is the most oxidized two-carbon compound. It is made in high concentrations by some plants and fungi and can reach high micromolar concentrations in soil (4). Oxalate is toxic to mammals but is metabolized by many bacteria and plants by various pathways. In *Oxalobacter formigenes*, oxalate is first activated to oxalyl-CoA and then decarboxylated, giving formyl-CoA and CO_2. Formyl-CoA transferase then exchanges the formyl group for an oxalyl-group on CoA, thus producing formate and regenerating oxalyl-CoA. Energy for growth on oxalate in *O. formigenes* results from a formate-oxalate antiporter, which generates an electrochemical transmembrane gradient for ATP synthesis (5, 6), so most formate produced is excreted rather than oxidized (7). Other organisms, such as *Cupriavidus oxalaticus*, also use oxalyl-CoA decarboxylase to metabolize oxalate but use formate dehydrogenase to generate NADH with the electrons derived from oxalate (8, 9). Oxalyl-CoA decarboxylase is a TPP-dependent enzyme with distant homology to yeast pyruvate decarboxylases (10). The *M. thermoacetica* genome has sequences with low homology to oxalyl-CoA decarboxylase but no homolog of formyl-CoA transferase. In fungi and in some bacteria, including *Bacillus subtilis*, oxalate can also be metabolized by oxalate decarboxylase, a manganese-containing cupin family protein, to generate formate and CO_2 (11). This reaction requires O_2. Another Mn^{2+}-cupin called germin that is found in plants catalyzes the oxidative decarboxylation of oxalate in the reaction $C_2O_4^{2-} + 2H^+ + O_2 \rightarrow 2CO_2 + H_2O_2$ (12). No enzyme that catalyzes anaerobic oxalate oxidation has been reported previously.

During growth on oxalate, *M. thermoacetica* consumes 4 mol of oxalate to produce 1 mol of acetate and 6 mol of CO_2 (Reaction 1) (13).

* This work was supported, in whole or in part, by National Institutes of Health (NIH) Grant GM39451 (to S. W. R.) and NIH, NCRR, Grant P20 RR-017675 (to D. F. B.) (for the ultracentrifugation studies). This work was also supported by National Science Foundation Grant DBI-0619764.

[S] The on-line version of this article (available at http://www.jbc.org) contains supplemental Figs. S1–S5 and Table S1.

[1] To whom correspondence should be addressed: Dept. of Biological Chemistry, University of Michigan, University of Michigan Medical School, 5301 MSRB III, 1150 W. Medical Center Dr., Ann Arbor, MI 48109-0606. Tel.: 734-615-4621; Fax: 734-763-4581; E-mail: sragsdal@umich.edu.

$$4\ C_2O_4^{-2} + 5\ H_2O \rightarrow CH_3COO^- + 6\ HCO_3^- + OH^- \ (\Delta G = -41.4\ \text{kJ/mol oxalate})$$

REACTION 1

Two proteins (33 and 42 kDa) were identified as being induced when *M. thermoacetica* was exposed to oxalate (14). Similarly, Daniel *et al.* (14) found that oxalate-grown cells metabolize oxalate much more quickly than cells that had been grown on glucose, which is consistent with an oxalate induction mechanism (15). They also showed that cell extracts from oxalate-grown cells could catalyze oxalate-dependent benzyl viologen reduction, that this activity was only slightly stimulated by coenzyme A, and that the electron acceptor specificity of oxalate oxidation was different than that of formate oxidation. They concluded that *M. thermoacetica* catabolizes oxalate by a CoA-independent mechanism that does not use formate as an intermediate.

This paper describes the characterization of the oxalate-induced enzyme, oxalate oxidoreductase (OOR)[2] and demonstrates that it, unlike all previously characterized members of the thiamine pyrophosphate (TPP)-dependent 2-oxoacid:ferredoxin oxidoreductase family, does not require coenzyme A. Coupling OOR to the Wood-Ljungdahl pathway allows anaerobic bacteria to generate energy by converting oxalate to acetyl-CoA.

EXPERIMENTAL PROCEDURES

Culture Media and Growth Conditions—M. thermoacetica ATCC 39073 was grown at 55 °C in stoppered, crimp-sealed 120-ml serum bottles pressurized with pure CO_2 and containing 100 ml of medium, or in a 10-liter fermentor that was continually bubbled with CO_2 during growth. The medium was modified from the "undefined medium" of Lundie and Drake (16) and contained 5 g/liter yeast extract, 5 g/liter tryptone, 0.1 mM $Fe(NH_4)_2(SO_4)_2$, 4.4 mM sodium thioglycolate, 7.6 mM $(NH_4)_2SO_4$, 1.0 mM $MgSO_4$, 0.2 mM $CaCl_2$, 0.1 mM $CoCl_2$, 20 μM $NiCl_2$, 6.8 mM NaCl, 0.1 mM nitrilotriacetic acid, 5 μM $ZnCl_2$, 7 μM Na_2SeO_3, 3 μM Na_2WO_4, 25 μM Na_2MoO_4, 25 μM $MnCl_2$, 2.4 μM H_3BO_2, and 0.3 μM $KAl(SO_4)_2$ (solution A) and 20 mM K_2HPO_4, 100 mM $NaHCO_3$ and 20 mM KH_2PO_4 (solution B). Solutions A and B were autoclaved separately, combined after cooling, and sparged with CO_2. Before inoculation, the medium was supplemented with glucose (100 mM in 100-ml cultures, 20 mM in the fermentor) and/or oxalate (27 mM), a vitamin solution (16), and 10 ml/liter reducing solution (36 g/liter each of $Na_2S{\cdot}9H_2O$ and cysteine-HCl). Cells were harvested during exponential growth by centrifugation under CO_2 or N_2 and were stored at −80 °C until use.

Two-dimensional Gel Electrophoresis—For two-dimensional gel electrophoresis, proteins were extracted with phenol as described (17), except that instead of tissue grinding, sonication was used to break the cells and, after precipitation of proteins in methanol, the protein pellet was washed twice with ice-cold acetone (80% in water) and once with ice-cold ethanol (70% in water). After washing, the protein pellets were suspended in 8 M urea, 2 M thiourea, 2% (w/v) CHAPS, 2% (w/v) Triton X-100, and 50 mM dithiothreitol (DTT) to ~1 μg/μl protein. Samples (150 μl) were supplemented with Bio-Lyte ampholytes (Bio-Rad) and loaded on 7-cm Bio-Rad isoelectric focusing gel strips (gradient from pH 5 to 8). The gels were subjected to a 12-h rehydration at 50 V, followed by focusing at 250 V for 15 min and then at 4000 V for 35,000 V-h. After isoelectric focusing, the isoelectric focusing gel strips were soaked in 6 M urea, 2% (w/v) SDS, 0.375 M Tris-HCl, pH 8.8, 20% (w/v) glycerol, and 20 mg/ml DTT for 15 min, followed by incubation for 15 min in the same buffer but with 25 mg/ml iodoacetamide instead of DTT. Strips were rinsed in running buffer before loading them at the top of 12.5% acrylamide gels for SDS-PAGE. After SDS-PAGE, proteins were stained with Coomassie Blue. Spots were cut from the gels, and proteins were identified by mass spectrometry at the University of Michigan Protein Structure Facility. A blank spot of each gel was also taken and processed. The samples were subjected to in-gel trypsin digestion. As a control, BSA was run on a separate gel and subjected to the same digestion and mass spectrometry procedure. LC-MS/MS was performed on a Q-TOF Premier mass spectrometer. Protein Lynx Global Server and Mascot search engines were used to search the SwissProt and NCBI databases.

Purification of OOR—Protein was purified from *M. thermoacetica* cells grown in the fermentor on glucose and oxalate. All purification steps and subsequent enzymatic manipulations were done in a Vacuum Atmospheres (Hawthorne, CA) anaerobic chamber maintained at ≤4 ppm O_2. Cells were suspended in Buffer A (50 mM Tris-HCl, 2 mM $MgCl_2$, 2 mM DTT, 1 mM TPP, pH 7.9) with 0.25 mg/ml lysozyme and 0.2 mM phenylmethanesulfonyl fluoride, sonicated, and centrifuged at 4 °C at 100,000 × *g* for 1 h. The supernatant was loaded on a 5 × 25-cm DEAE-cellulose column, and proteins were eluted with a gradient from 0.1 to 0.5 M in Buffer A. The 0.3 M fraction was diluted to 0.075 M NaCl with Buffer A and loaded on a 2.5 × 25-cm red agarose (Sigma-Aldrich) column. OOR did not bind to this column, so 0.85 M ammonium sulfate was added to the flow-through and wash fractions, and these were loaded on a 2.5 × 25-cm fast flow high substitution phenyl-Sepharose (GE Healthcare) column and eluted with a reverse linear gradient from 0.85 to 0 M ammonium sulfate and 10% glycerol in Buffer A. Oxalate oxidation activity eluted at around 0.45 M ammonium sulfate. Fractions containing OOR activity were pooled, concentrated, and exchanged into Buffer A using 30-kDa molecular mass cut-off centrifuge concentrators. The protein was loaded on a 2.5 × 25-cm high performance Q-Sepharose column (Sigma-Aldrich) and eluted with a linear gradient from 0 to 0.7 M NaCl in Buffer A. OOR activity eluted at 0.47 M NaCl. Fractions containing OOR activity were pooled and exchanged into 50 mM Tris-HCl, pH 7.9, and 2 mM DTT. OOR was stored in 50 mM Tris-HCl, pH 7.9, and 2 mM DTT at a concentration of 210 μM, and dilutions of this protein stock were

[2] The abbreviations used are: OOR, oxalate oxidoreductase; OFOR, 2-oxoacid:ferredoxin oxidoreductase; Fd, ferredoxin; PFOR, pyruvate:ferredoxin oxidoreductase; CODH, CO dehydrogenase; TPP, thiamine pyrophosphate; ACS, acetyl-CoA synthase; BisTris, 2-[bis(2-hydroxyethyl)-amino]-2-(hydroxymethyl)propane-1,3-diol.

used for all subsequent experiments unless described otherwise.

Enzyme Assays—OOR activity was measured in 50 mM Tris-HCl, 2 mM DTT, pH 7.9. Assays at 25 °C were done in a Vacuum Atmospheres anaerobic chamber maintained at ≤4 ppm O_2, using a UV-visible spectrophotometer from Ocean Optics (Dunedin, FL). Assays at 40 or 55 °C were performed in stoppered cuvettes flushed with N_2 gas, in an OLIS (Bogart, GA)-modified Cary-14 spectrophotometer. For steady-state assays performed with saturating substrate concentrations, 1 mM sodium oxalate and 10 mM methyl viologen were used, and the reduction of methyl viologen was followed at 578 nm (ϵ_{578} = 9.7 mM^{-1} cm^{-1}). In assays using ferredoxin ($\Delta\epsilon_{420}$ = 7.5 mM^{-1} cm^{-1}), horse heart cytochrome *c* ($\Delta\epsilon_{553}$ = 19.4 mM^{-1} cm^{-1}), NAD^+ or $NADP^+$ (ϵ_{340} = 6.22 mM^{-1} cm^{-1}), FMN (ϵ_{450} = 12.2 mM^{-1} cm^{-1}), FAD (ϵ_{450} = 11.3 mM^{-1} cm^{-1}), or CO dehydrogenase (CODH), methyl viologen was omitted. The extinction coefficients for FMN and FAD are for two-electron reductions. The $\Delta\epsilon_{320}$ for metronidazole was determined by titrating 100 μM metronidazole with 20 μM aliquots of oxalate, in the presence of 1.8 μM OOR ($\Delta\epsilon_{320}$ = 3.2 (mM reducing equivalent)$^{-1}$ cm^{-1}) at 320 nm. In all assays, calculations were based on the assumption that oxidation of 1 mol of oxalate produces 2 mol of electrons. CODH as an electron acceptor for OOR was assayed in 50 mM sodium phosphate, pH 7.0, with 1 mM oxalate, 20 μM CODH/acetyl-CoA synthase (ACS) from *M. thermoacetica*, and 50 μM myoglobin in stoppered cuvettes that were flushed with 20% CO_2, 80% N_2 (6.8 mM CO_2 in solution). The stock solution of myoglobin was prereduced by adding a stoichiometric amount of sodium dithionite. Formation of CO from CO_2 was measured as myoglobin-bound CO. At pH 7, the specific activity of CO_2 reduction by CODH using dithionite (instead of OOR) as a reductant was 4.7 μmol min^{-1} μmol $CODH^{-1}$. Formation of myoglobin-CO was monitored at 423 nm. The extinction coefficient, $\Delta\epsilon_{423}$ = 129 mM^{-1} cm^{-1}, was determined from the difference between the spectra of myoglobin-CO and dithionite-reduced myoglobin. The concentration of myoglobin used for these spectra was determined from extinction coefficients of 121 mM^{-1} cm^{-1} at 435 nm for ferrous myoglobin and 207 mM^{-1} cm^{-1} at 423 nm for myoglobin-CO (18).

For whole cell assays, cells were harvested from growing cultures, washed twice with 15 mM NaCl in 50 mM potassium phosphate, pH 7.0, and resuspended in stoppered serum bottles in fresh growth medium with 10 mM oxalate and 1 atmosphere of CO_2. Aliquots were removed with a syringe and quenched in 1 M HCl, and oxalate concentrations were measured by HPLC on a 300 × 7.8 mm Bio-Rad Aminex HPX-87H column with a mobile phase of 0.008 N H_2SO_4 in a Beckman Coulter (Brea, CA) System Gold HPLC with diode array UV-visible detector. Oxalate was detected by its absorbance at 210 nm. Concentrations were determined by comparison with oxalate standards prepared in the medium used for the assays. Oxalate concentrations between 0.25 and 10 mM could be reliably determined by this assay. HPLC-based assays with purified protein or cell extracts were performed in the same way, except that 50 mM Tris-HCl, pH 8.0, with 10 mM oxalate and 10 mM methyl viologen (under an N_2 atmosphere) was used instead of growth medium, and oxalate standards were prepared in the assay buffer.

The pH dependence of OOR activity was determined by measuring activity with 1 mM oxalate and 10 mM methyl viologen in 50 mM buffer containing 2 mM DTT. Buffers were made by mixing 50 mM solutions of conjugate acid and base in different proportions, and the pH of each buffer and DTT solution was measured before starting each assay. The buffers used were MES (pK_a = 6.02, used from pH 5.0 to 7.1), sodium phosphate (pK_a = 6.82, used from pH 5.9 to 7.8), borate (pK_a = 8.94, used from pH 8.1 to 9.1), and *N*-cyclohexyl-3-amino-propanesulfonic acid (pK_a = 9.42, used from pH 8.4 to 10.2).

UV-visible Spectroscopy—OOR was diluted to 4.1 μM in 50 mM Tris-HCl, pH 7.9, and 2 mM DTT to measure the UV-visible spectrum of the as-isolated protein. The enzyme was reduced at 25 °C by adding 100 μM sodium oxalate. To measure the spectrum of the oxidized protein, 4.1 μM OOR was mixed with 50 nM *M. thermoacetica* CODH/ACS in 50 mM potassium phosphate, pH 7.0. The cuvette containing this mixture was stoppered, and the headspace was flushed with 20% CO_2, 80% N_2. After 5 min of CO_2 exposure, the spectrum was recorded. In this reaction, electrons from OOR are transferred to CODH, which reduces the CO_2 to CO. Once OOR was fully oxidized, the spectrum did not change during another 1 h of CO_2 exposure.

EPR Spectroscopy—OOR was concentrated and diluted in 50 mM Tris-HCl, pH 8.0 (without DTT), to a concentration of 49 μM. Comparison of the UV-visible spectrum of this protein with dithionite-reduced OOR showed that the protein was two-thirds reduced. Sodium oxalate (50 μM, final) was added to completely reduce the protein. After reduction, different amounts of horse heart cytochrome *c* and 50 mM Tris-HCl, pH 8.0, were added to generate samples that were 39 μM OOR and between 20 and 160 μM cytochrome *c*. EPR spectra were collected at 9 K, and the parameters were as follows: receiver gain, 2×10^2; modulation frequency, 100 kHz; modulation amplitude, 10 G; center field, 3450 or 3500 G; sweep width, 700 or 2000 G; microwave power, 0.129 milliwatt. The double integrals of the EPR signals were compared with that of a 1 mM copper(II) perchlorate standard to determine the number of spins per monomeric unit.

Size Exclusion Chromatography—A 90 × 1.6-cm column of Superdex 200 resin (GE Healthcare) was equilibrated with an anaerobically prepared solution of 50 mM Tris-HCl, pH 8.1, with 2 mM DTT, 0.2 mM $Na_2S_2O_4$, and 0.5 mM sodium oxalate. The buffer was added to the column through a continuous closed system of tubing, and the bottle containing the buffer was closed by a rubber stopper and pressurized with N_2 gas during use to keep O_2 from entering the buffer and column. Proteins were anaerobically dissolved in the same buffer, removed from the anaerobic chamber in stoppered serum vials, and added to the column sample loop with a Hamilton gas-tight syringe. Blue dextran; a standard protein mixture consisting of carbonic anhydrase (29 kDa), bovine serum albumin (66 kDa), alcohol dehydrogenase (150 kDa), β-amylase (200 kDa), apoferritin (443 kDa), and thyroglobulin

(669 kDa); OOR; and *M. thermoacetica* pyruvate ferredoxin oxidoreductase were run separately over the column. Blue dextran and standard proteins were purchased from Sigma-Aldrich.

Sedimentation Equilibrium—The oligomeric state of OOR was determined at 20 °C by sedimentation equilibrium under anaerobic conditions using an Optima XL-I analytical ultracentrifuge (Beckman Coulter, Inc.) equipped with an eight-hole An50 Ti rotor. OOR was dialyzed against 50 mM Tris-sulfate buffer (pH 8.0) containing 2 mM DTT and 100 mM NaCl before centrifugation. Sample and reference cells were incubated overnight in an anaerobic glove box (nitrogen atmosphere; Belle Technology) prior to loading with reference buffer and OOR samples. Three concentrations (8.3, 21, and 32 μM) of OOR were loaded (110 μl) in the sample cells, and the reference cells were filled with the dialysate buffer (125 μl). Radial scans were collected at 430, 460, and 470 nm after 22 and 24 h using a rotor speed of 6000 rpm. The scans are an average of 10 measurements at each radial position with a spacing of 0.001 cm. Data were fit by global analysis to an equation describing a single-species model using Origin 6.0. The partial specific volume of OOR used for best fit analysis was 0.7396, which is the average of the three OOR polypeptides calculated by SedTerp. The solvent density of the buffer was calculated to be 1.0038 g/ml.

Miscellaneous Methods—The stoichiometry of the three OOR peptides was estimated from a Coomassie-stained SDS-polyacrylamide gel of the purified protein. To find the relative amounts of the three bands, the gel was scanned and digitized using UN-SCAN-IT gel Version 6.1 software from Silk Scientific (Orem, UT). Blue native polyacrylamide gel electrophoresis was done with the Invitrogen NativePAGE Novex BisTris gel system, using 4–16% acrylamide gradient gels, and NativeMark protein standards. OOR and PFOR proteins were mixed with 0.5% Coomassie G-250 before loading gels. Protein concentrations were determined by the rose bengal method (19), using a lysozyme standard. The concentration of TPP bound to OOR was determined by a fluorescent thiochrome assay (20). Pure TPP was used as a standard. Metal concentrations were determined by ICP-OES at the Chemical Analysis Laboratory at the University of Georgia. For metal analysis, 1.1 ml of 20 μM OOR was dialyzed against two changes of 500 ml of 100 mM Tris-HCl, 2 mM DTT, pH 7.9. Metal concentrations in the protein sample were calculated after subtracting the concentrations in a sample of the dialysis buffer treated exactly as was the protein.

RESULTS

Identification of Proteins Induced during Growth of M. thermoacetica on Oxalate—Daniel and Drake (14) showed by SDS-PAGE that 33- and 42-kDa proteins are induced during growth of *M. thermoacetica* on oxalate. Cell extracts from cells grown with different substrates, SDS-PAGE (supplemental Fig. S1, *lanes 2* and *3*), and two-dimensional electrophoresis (supplemental Fig. S2) experiments reveal three proteins (with molecular masses of 42, 39, and 35 kDa) that are more strongly expressed in cells grown in stoppered culture flasks on oxalate or on oxalate and glucose than those grown on glucose (in the absence of oxalate). These three proteins were identified by mass spectrometry as the subunits of an annotated 2-oxoacid:ferredoxin oxidoreductase, with NCBI accession numbers of YP_430440, YP_430441, and YP_430442 and Joint Genome Institute locus tag classifications Moth_1593, Moth_1592, and Moth_1591, respectively (21) (supplemental Table S1). Directly upstream from Moth_1593 are two genes that are transcribed in the same direction, which encode a transcriptional regulator (Moth_1595) and an AAA family ATPase in the CDC48 subfamily (Moth_1594). The N-terminal domain of the predicted transcriptional regulator is annotated as a GntR family helix-turn-helix pfam domain, and the C-terminal domain is annotated as an FCD ligand-binding domain. Moth_1590, downstream from Moth_1591, encodes a major facilitator superfamily protein with 35% sequence identity to the oxalate-formate antiporter of *O. formigenes* (22) (supplemental Fig. S3).

Purification of Oxalate-degrading Activity from M. thermoacetica—As shown earlier (15), we found that cell extracts containing soluble protein from *M. thermoacetica* grown on oxalate and glucose catalyzed oxalate-dependent reduction of methyl viologen. Based on an HPLC-based assay that measures the decrease in oxalate concentration, the OOR specific activity was 0.4 μmol min^{-1} mg protein^{-1} at 55 °C, whereas that of extracts from cells grown on glucose without oxalate was less than 0.03 μmol min^{-1} mg protein^{-1} at 55 °C. We also used the HPLC-based assay to measure oxalate degradation by whole cells of *M. thermoacetica* grown on oxalate and glucose or on glucose alone. In these assays, which were followed for several h, oxalate was degraded 30 times more quickly by cells that had been previously exposed to oxalate than by cells grown on glucose without oxalate.

To determine if the 2-oxoacid:ferredoxin oxidoreductase homolog that is overexpressed during growth on oxalate is the only protein needed for the oxalate-dependent methyl viologen reducing activity seen in cell extracts, we purified OOR from *M. thermoacetica* cells to greater than 95% purity, as shown by SDS-PAGE (Fig. 1 and Table 1). After 22-fold purification, the active protein consisted of three peptides in 1:0.8:1 stoichiometry, with estimated sizes of 36, 43, and 32 kDa, which corresponds well to the predicted masses of 34.2, 43.7, and 33.9 kDa for YP_430440, YP_430441, and YP_430442. The purified OOR preparation retained 0.015 unit/mg of CODH activity, indicating that there is a 0.03% contamination of OOR with CODH/ACS, which apparently was not completely separated from the OOR during the purification procedure.

When run on blue native polyacrylamide gel electrophoresis, most of the protein was found in a major band with an estimated molecular mass of 243 kDa and another species with a mass of 445 kDa (supplemental Fig. S1). Molecular exclusion chromatographic analysis of OOR reveals predominantly a 236-kDa species and a 117-kDa species, which accounts for 10–20% of the total protein (supplemental Fig. S4). In a parallel gel filtration experiment, the *M. thermoacetica* PFOR was shown to elute with a similar profile. The quaternary structure of OOR was also characterized by analytical ultracentrifugation. Fig. 2 shows the results from sedimenta-

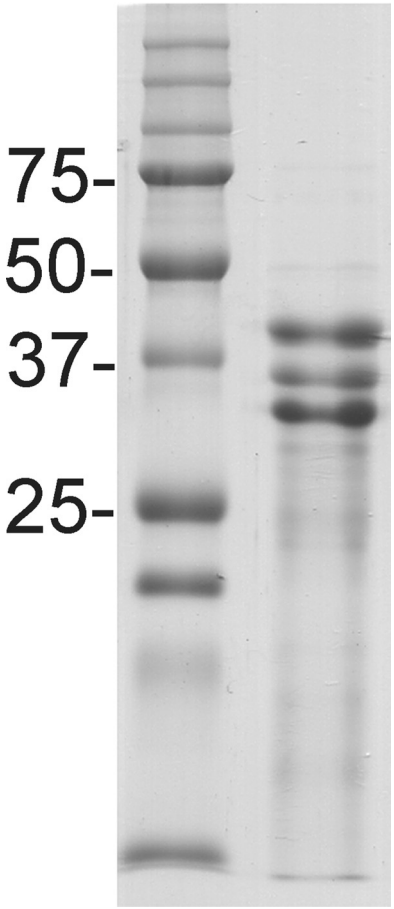

FIGURE 1. **SDS-PAGE of purified OOR.** *Left lane*, molecular mass marker (sizes shown in kDa); *right lane*, 6 μg of purified OOR.

TABLE 1
Purification of OOR

Purification step	Amount[a]	Protein	Total	Purification
	units/mg	*mg*	*units*	*-fold*
Cell-free extract	0.009	3780	34	1
DEAE-cellulose	0.044	1590	70	5
Phenyl-Sepharose	0.169	349	54	18
Q-Sepharose	0.200	108	22	22

[a] Measured at 40 °C.

tion equilibrium analysis of OOR at three different concentrations. A best fit value of 226,890 Da was estimated for the molecular mass of OOR which is within 1.5% of the molecular mass predicted for a dimeric species (223,700 Da). These combined results indicate that, like PFOR and other OFORs, OOR forms a dimeric structure consisting of two heterotrimeric units.

Sequence Analysis of OOR—2-oxoacid:ferredoxin oxidoreductases are made up of a minimum of three conserved domains, α, β, and γ, with an additional δ domain in most OFORs. The genomic arrangement and fusion of these domains varies. The residues involved in binding TPP and one $[Fe_4S_4]^{2+/1+}$ cluster are in the β subunit (23). Enzymes that include the δ subunit have two additional $[Fe_4S_4]^{2+/1+}$ clusters that are involved in electron transfer from the TPP active site to ferredoxin (24).

The OOR protein is made up of separate α and β subunits and a third subunit that is a fusion of γ and δ domains (Fig. 3).

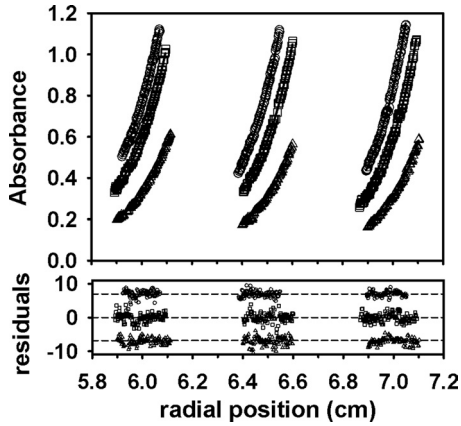

FIGURE 2. **Sedimentation equilibrium analysis of OOR.** The *top panel* shows a global fit of analytical ultracentrifugation data for three different concentrations of OOR collected at 6000 rpm. Absorbance data were recorded at 430, 460, and 470 nm for 8.3 μM (*triangles*), 20.7 μM (*squares*), and 32.3 μM (*circles*) OOR concentrations, respectively. The *solid line* through the points is the weighted best least squares fit to an ideal single-species model. Residuals for each fit are shown in the *bottom panel*. A vertical offset was applied to the residuals from the 8.3 μM (*triangles*) and 32.3 μM (*circles*) concentrations for clarity.

We performed separate ClustalW alignments of the sequences of the three OOR subunits with those of corresponding subunits of biochemically characterized pyruvate, 2-oxoisovalerate, 2-oxoglutarate, indole pyruvate, and broad specificity oxidoreductases (see legend to supplemental Fig. S4). The chosen sequences included the *Desulfovibrio africanus* PFOR, which has been crystallized in complex with pyruvate (25), allowing us to determine whether or not oxoacid binding residues are conserved in OOR. In the β subunit, residues that coordinate TPP, the adjacent Mg^{2+} ion of the $[Fe_4S_4]$ cluster that is nearest TPP, are conserved. The eight cysteine residues that bind the other two $[Fe_4S_4]$ clusters are conserved in the OOR δ subunit.

In the α and β subunits, two of five substrate-binding residues from *D. africanus* PFOR are conserved in OOR. Arg 109 corresponds to Arg^{114} in *D. africanus* PFOR, which binds the carboxyl group of pyruvate. Three other residues, Ile^{123}, Ile^{843}, and Asn^{996}, are less strongly conserved among the other OFORS. In the *D. africanus* PFOR structure, Asn^{996} forms a hydrogen bond to the carbonyl group, and Ile^{843} and Ile^{123} interact with the methyl group of pyruvate. The corresponding residues are Asn^{143} and Val^{55} in the β subunit and Phe^{117} in the α subunit of OOR. The fifth residue, Thr^{31} in PFOR, is part of a strongly conserved YPITP motif that is present in OFORs using many different substrates (26) and is within hydrogen bonding distance of the α-keto oxygen of pyruvate in the *D. africanus* PFOR crystal structure. This Thr residue is replaced by Arg in the OOR sequence (supplemental Fig. S5), thus forming a YPIRP motif. A BLAST search of the non-redundant protein data base at NCBI shows that this substitiution is rare; eight of the 11 sequences most closely related to OOR have Thr^{31} replaced with arginine, but no other sequence in the first 500 BLAST hits has arginine in this position.

Cofactor Binding—OOR was purified in buffer containing 1 mM TPP and 2 mM $MgCl_2$, and, during the purification, the

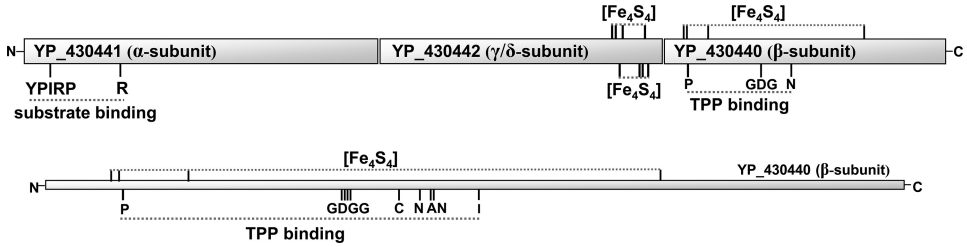

FIGURE 3. **Schematic of OOR peptides.** *Top*, arrangement of the three peptide sequences as they align with pyruvate:ferredoxin oxidoreductases from *D. africanus* and *M. thermoacetica*. Each *rectangle* represents a separate gene product. Locations of conserved residues that may be involved in iron-sulfur cluster, TPP, Mg^{2+}, and substrate binding are shown. All residues proposed to ligate the $[Fe_4S_4]$ clusters are cysteines. *Bottom*, expanded view of the β subunit of OOR showing both conserved and non-conserved residues that align with the $[Fe_4S_4]$ cluster and TPP-binding residues of *D. africanus* PFOR.

TABLE 2
Cofactor content of OOR

Metal or co-factor	As-isolated OOR	Dialyzed OOR
	mol/mol protein	
TPP	1.03	0.71
Iron	14.0	14.3
Magnesium	1.9	0.8
Sodium	24.3	6.1
Potassium	1.0	8.3
Calcium	0.6	1.8

protein was assayed in the same buffer. After purification, the protein was exchanged into 50 mM Tris-HCl with 2 mM DTT but without TPP or $MgCl_2$. The activity of the protein did not change after buffer exchange, and we found that it was not necessary to add TPP to assays to see full activity. Using a fluorescent assay to quantify thiochrome bound to OOR, 1.0 mol of TPP were found per mol of protein.

As-isolated OOR is brown; metal analysis by ICP showed 14 mol of iron and 0.8 mol of Mg^{2+} per mol of protein. After preparing the protein for metal analysis by dialysis into metal-free buffer, the protein retained activity with 0.7 mol of TPP/mol of protein. Mg^{2+} is likely to help with TPP binding as it does in other TPP-dependent enzymes. Calcium, sodium, and potassium were also present in the sample in greater than stoichiometric amounts, but their concentrations varied widely between two metal analysis samples, so it is possible that they bind nonspecifically to the protein (Table 2).

Catalytic Properties of OOR—The purified heterotrimeric protein catalyzed the oxidation of oxalate using methyl viologen as an electron acceptor with a specific activity of 0.05 μmol min^{-1} mg^{-1} (k_{cat} = 0.095 s^{-1} at pH 7.9) and a K_m for oxalate of 58 ± 6 μM (Fig. 4*A*). The addition of CoA from 1 μM to 1 mM had no effect on the OOR reaction rate (Fig. 4*A*). In addition, the addition of 1 mM ATP and 1 mM CoA together to the assay mixture did not affect the rate of the reaction. The pH dependence of OOR activity was measured at pH values between 5.0 and 10.2 using saturating concentrations of oxalate (1 mM). The maximum activity (0.11 unit/mg, 0.21 s^{-1}) was observed at pH 8.7 (Fig. 4*B*). Other reported optimal pH values for activity of 2-oxoacid:Fd oxidoreductases are between pH 7.5 and 9.0 (27–33). Because the pK_a values for oxalate are 1.23 and 4.19 (34), the fully deprotonated form would be the substrate at the optimal pH for OOR.

OOR showed slow activity with all 2-oxoacids tested (Table 3). The OOR preparation had no formate dehydrogenase activity, which indicates that the decarboxylase activity of OOR, like other OFORs, is strictly coupled to electron carrier reduction, unlike the decarboxylases, where the electron pair is retained in the other product (*e.g.* pyruvate decarboxylase generates CO_2 and acetaldehyde). These results are consistent with earlier assays of cell lysates (15), in which it was shown that the oxalate-catabolizing system in *M. thermoacetica* had different electron acceptor specificity than formate dehydrogenase. OOR was active with a broad range of electron acceptors (Table 4). OOR used CODH as an electron acceptor, catalyzing the oxalate-dependent reduction of CO_2 to CO.

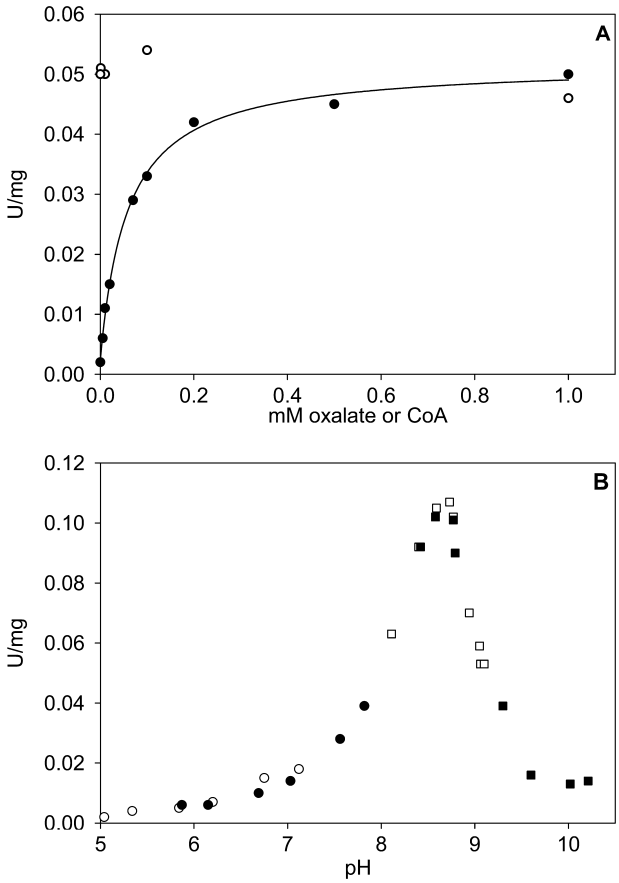

FIGURE 4. **Oxalate and pH dependence of OOR activity.** *A*, activity was measured at 25 °C in 50 mM Tris-HCl, pH 7.9, with 10 mM methyl viologen and with varying oxalate concentrations (*closed circles*) or 1 mM oxalate and varying coenzyme A concentrations (*open circles*). *B*, activity was measured at 25 °C in MES (*open circles*), sodium phosphate (*closed circles*), borate (*open squares*), and *N*-cyclohexyl-3-amino-propanesulfonic acid (*closed squares*).

Spectral Characterization of OOR—The UV-visible spectrum of as-isolated OOR had a broad absorbance shoulder between 300 and 500 nm (Fig. 5). The absorbance in this re-

TABLE 3
Substrate specificity of OOR

Substrate	Activity
	$\mu mol\ min^{-1}\ mg^{-1}$
Oxalate	0.049 ± 0.004
Glyoxylate	0.024 ± 0.006
Glyoxylate + 100 μM CoA	0.029 ± 0.007
Pyruvate	0.005 ± 0.001
Pyruvate + 100 μM CoA	0.005 ± 0.001
2-Oxobutyrate	0.014 ± 0.001
Oxaloacetate	0.007 ± 0.003
2-Oxovalerate	0.003 ± 0.001
2-Oxoglutarate	0.004 ± 0.002
Formate	ND[a]

[a] ND, not detected. Slow enzyme-dependent methyl viologen reduction of about 0.002 unit/mg was seen in assays with no substrate, so we could not measure any slower activity.

TABLE 4
Electron acceptor specificity of OOR

Electron acceptor	Activity
	$\mu mol\ min^{-1}\ mg^{-1}$
Methyl viologen (20 μM)	0.047 ± 0.008
Metronidazole (20 μM)	0.014 ± 0.002
Ferredoxin (20 μM)	0.029 ± 0.001
Cytochrome *c* (20 μM)	0.182 ± 0.004
NAD^+ (20 μM or 1 mM)	ND[a]
$NADP^+$ (20 μM or 1 mM)	ND
FAD (20 μM)	0.049 ± 0.008
FMN (20 μM)	0.057 ± 0.004
CODH (20 μM)	0.006 ± 0.001[b]

[a] ND, not detected with 230 μg of enzyme in a 1-ml assay.
[b] Measured at pH 7.0, where CO_2 reduction by CODH with dithionite as a reductant was 4.7 $\mu mol\ min^{-1}$ $\mu mol\ CODH^{-1}$. OOR activity is approximately 3-fold less at pH 7 than at pH 8 with methyl viologen as electron acceptor, and OOR is inhibited by CO_2, with approximately half as much activity under 6.8 mM CO_2 as with no CO_2.

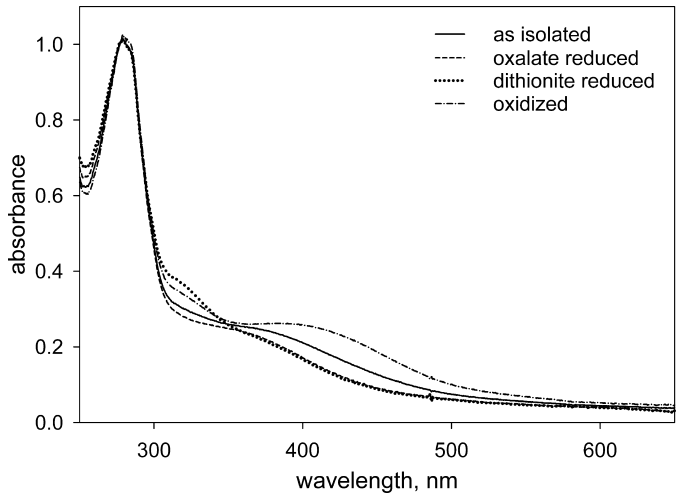

FIGURE 5. **UV-visible spectra of OOR.** *Solid line*, as-isolated protein; *dashes* and *dots*, oxidized protein; *short dashes*, oxalate-reduced protein; *dots*, dithionite-reduced protein. Spectra were measured anaerobically. 4.1 μM protein was prepared in 50 mM sodium phosphate, pH 7.0. Reduced protein was prepared by adding 10 μM sodium oxalate or 15 μM sodium dithionite to the as-isolated protein sample, and the spectra shown were recorded after 20 min. Oxidized protein was prepared by incubation in 6.8 mM CO_2 with 80 nM CODH/ACS from *M. thermoacetica*.

gion increased when the protein was exposed to air or treated with ferricyanide. Treating the protein with sodium dithionite decreased the absorbance of the band between 300 and 500 nm, which is consistent with the bleaching seen upon reduction of $[Fe_4S_4]^{2+/1+}$ clusters in other proteins (*e.g.* PFOR) (24). OOR is expected to bind three $[Fe_4S_4]$ clusters, based on

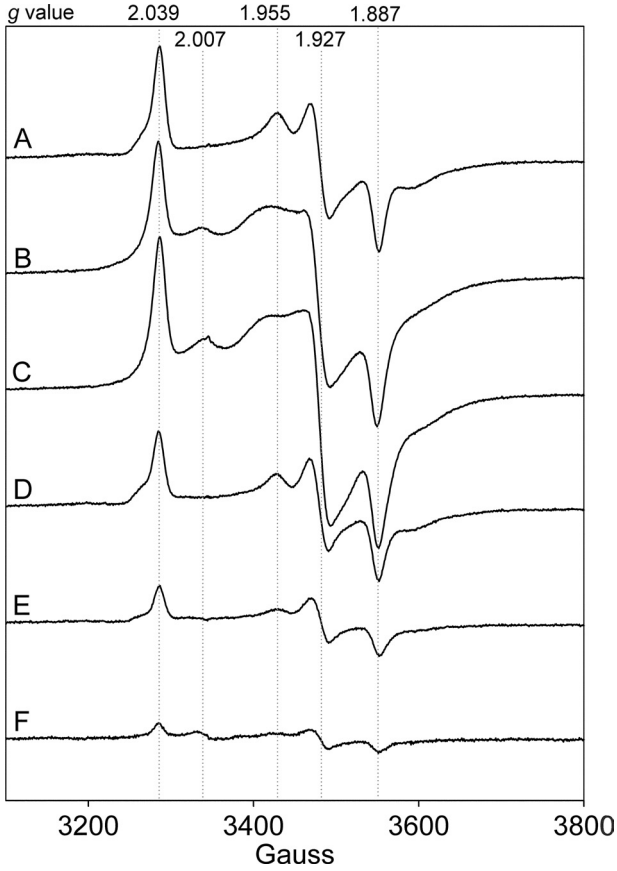

FIGURE 6. **EPR spectra of OOR.** 39 μM OOR was reduced with oxalate and then titrated with oxidized cytochrome *c*. *A*, as-isolated OOR (1.2 spins/monomer); *B*, oxalate-reduced OOR (3.4 spins/monomer); *C*, dithionite-reduced OOR (3.2 spins/monomer); *D–F*, oxalate reduced OOR, reoxidized by the addition of oxidized cytochrome *c* (*D*, 1.3 spins/monomer, *E*, 0.7 spins/monomer, *F*, 0.07 spins/monomer). The parameters were as follows: receiver gain, 2×10^2; modulation frequency, 100 kHz; modulation amplitude, 10 G; center field, 3450 G; sweep width, 700 G; microwave power, 0.129 milliwatt at 9 K.

the sequence alignments with PFOR and on the metal analyses described above. The maximum difference in absorbance between the oxidized and reduced protein was at 420 nm with a difference extinction coefficient ($\Delta\epsilon$) of 24.9 $mM^{-1}\ cm^{-1}$, or 8.3 per mM $[Fe_4S_4]$, which is similar to the extinction coefficients of 7–7.5 per mM cluster that have been reported for PFOR (24, 35). When OOR was incubated with oxalate, an identical difference spectrum was observed, and after oxalate reduction, OOR was oxidized by the addition of a catalytic amount of CODH/ACS and excess CO_2.

Because $[Fe_4S_4]$ clusters are diamagnetic in the oxidized (2+) state and paramagnetic in the reduced (1+) state, OOR was studied by EPR to follow reduction of the protein by oxalate. The UV-visible spectrum of the protein used in this experiment was used to calculate that the as-isolated protein had 1.7 clusters reduced. As-isolated OOR exhibited an EPR spectrum (Fig. 6) with g values of 2.039, 1.955, 1.927, 1.887, and 1.865 (1.2 spins/mol). When a stoichiometric amount of oxalate was added to the protein, the signal intensity increased to 3.4 spins/mol. The 1.955 and 1.865 features became broader, and an additional feature at g = 2.007 was seen in samples of fully reduced OOR prepared with oxalate or

dithionite (3.2 spins/mol). This EPR spectrum was saturated above 0.129 milliwatt at 9 K. The relative intensities of the 2.039 and 1.927 features decreased as the power was increased, although they were still present at 129 milliwatts. When oxalate-reduced OOR was oxidized by the additions of oxidized cytochrome *c*, there was no change in the overall shape of the EPR spectrum, even in the almost completely oxidized protein (0.07 spins/mol, Fig. 6*F*), indicating that the potentials of the iron-sulfur clusters are similar. The g values of the OOR spectra are typical of $[Fe_4S_4]^{2+/1+}$ clusters, such as those in eight iron (2-$[Fe_4S_4]$) ferredoxins (36, 37) and other OFOR enzymes (35, 38). As eight iron ferredoxins go from partially to fully reduced, an increase in complexity of the EPR spectrum is seen, which results from spin-spin interactions between two reduced $[Fe_4S_4]$ clusters. Similar coupling of clusters has been seen in PFOR (35), as well as spin-spin interaction between an $[Fe_4S_4]$ cluster and a substrate-derived radical in the active site (38). We did not see an increase in complexity with increasing reduction of OOR, nor did we see a substrate-derived radical when OOR was frozen ~30 s after mixing with oxalate.

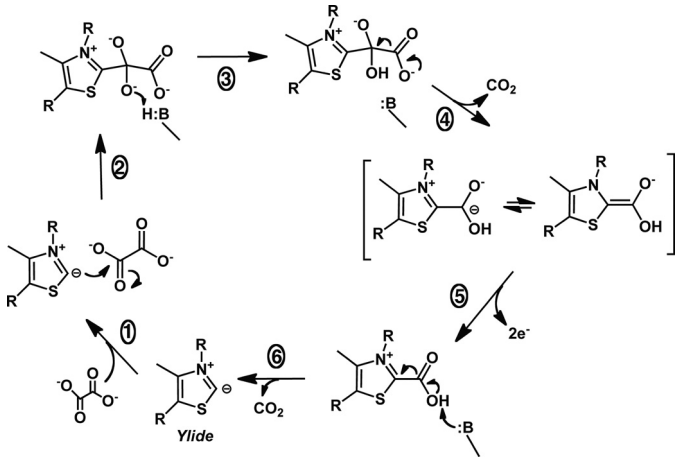

FIGURE 7. **Proposed OOR mechanism.** Oxalate binds to OOR (*step 1*) and undergoes nucleophilic attack by the TPP ylide (*step 2*), generating oxalyl-TPP, which could be stabilized by protonation from a general base (*step 3*). Decarboxylation (*step 4*) leaves an anionic intermediate that would release two electrons to the $[Fe_4S_4]$ clusters (*step 5*). The carboxyl-TPP that remains could be decarboxylated to release a second CO_2 molecule (*step 6*) or hydrolyzed to release bicarbonate (not shown), regenerating the starting form of the enzyme.

DISCUSSION

Oxalate is an important metabolite that is produced in the soil and in the animal gastrointestinal tract, with elevated levels causing kidney stones. Many bacteria that use oxalate as an energy source also use oxalate as a carbon source by reduction to glyoxylate, which is incorporated into the central metabolite 3-phosphoglycerate (39, 40), but enzymes involved in glyoxylate incorporation have not been detected in oxalate-grown cultures of *M. thermoacetica* (3, 13). We have shown that *M. thermoacetica* metabolizes oxalate very simply by a novel CoA-independent OFOR that catalyzes the oxidative decarboxylation of oxalate to 2 mol of CO_2, coupled to the reduction of ferredoxin (or other electron acceptors). The apparent reaction is $C_2O_4^{2-} + Fd_{ox} \leftrightarrow 2\ CO_2 + Fd^{i}_{red}$,[3] although we have not yet shown whether CO_2 or bicarbonate is the product that is released from OOR. Our results are consistent with previous studies, which indicate that incorporation of oxalate into cell material requires conversion to CO_2 (3, 14). For example, *M. thermoacetica* can grow on oxalate even in CO_2-free medium; however, when cells are grown on oxalate and CO_2, very little radioactivity from ^{14}C-oxalate is incorporated into biomass (14). Thus, OOR enables growth on oxalate by linking the production of CO_2 and reducing equivalents to the Wood-Ljungdahl pathway of autotrophic anaerobic acetyl-CoA formation (3, 14).

Oxalate induces the expression of three proteins (36, 43, and 32 kDa) in *M. thermoacetica* that can be resolved by two-dimensional PAGE. Earlier studies described the induction of two protein bands (one of the bands apparently was not resolved by one-dimensional SDS-PAGE) when *M. thermoacetica* was grown on oxalate, relative to growth on CO, formate, or glyoxylate (14). Genome-enabled mass spectrometric results reveal that the oxalate-induced proteins belong to the OFOR family and are encoded within an operon that includes a homolog of *O. formigenes* oxalate-formate antiporter, a permease and a gene encoding a transcriptional regulatory protein, for which we propose the name OorR. OorR contains an N-terminal helix-turn-helix DNA binding domain and a C-terminal ligand-binding domain and is likely to regulate expression of OOR and coordinate its expression with expression of the enzymes of the Wood-Ljungdahl pathway. Oxalate is a unique substrate for *M. thermoacetica*, which uses nitrate instead of CO_2 as an electron acceptor when grown on other multiple-carbon growth substrates in the presence of nitrate and CO_2. However, CO_2 is used preferentially over nitrate when it is growing on oxalate (3). Nitrate appears to inhibit autotrophic growth by repressing the Wood-Ljungdahl pathway at the transcriptional level (1, 2). We suggest that interactions between oxalate, OorR, and the promoters of the *oor* and *acs* operons are able to induce the *oor* operon and prevent the nitrate-dependent repression of the Wood-Ljungdahl pathway. *M. thermoacetica* does not produce formate from oxalate, but acetate, the end product of the Wood-Ljungdahl pathway, could be exchanged with oxalate by the antiporter.

OOR is the first protein shown to catalyze anaerobic oxalate oxidation, unlike previously described anaerobic enzymes that produce CO_2 and formyl-CoA (6, 9). Although several features (*e.g.* Fe_4S_4 clusters and TPP content) of OOR are similar to other members of the OFOR family, OOR is unique among family members in its lack of requirement for CoA. Fig. 7 shows a proposed mechanism of OOR, based on the results described here and on analogy with conserved features of other OFORs, such as PFOR, whose mechanism has been extensively studied (24, 35, 42) and whose crystal structure is known (25).

Steps 1 and 2: Binding of TPP, Mg^{2+}, and Oxalate—The early steps of the reaction would resemble those of all TPP-dependent enzymes, reviewed recently (43). After binding oxalate (step 1), step 2 of the proposed OOR mechanism in-

[3] The ferredoxin that we have used with OOR is an 8-Fe ferredoxin that contains two $[Fe_4S_4]$ clusters and accepts two electrons.

volves nucleophilic attack of the anionic ylide of OOR-bound TPP on oxalate to generate an oxalyl-TPP adduct. The purified OOR contains Mg^{2+} and TPP, which were added during purification because in some OFORs, like PFOR from *M. thermoacetica*, TPP dissociates rather easily, resulting in loss of activity in buffer lacking TPP. However, TPP remains tightly bound to OOR even after extensive buffer exchange and over several months' storage. Based on sequence homology between OOR and the *D. africanus* PFOR, whose structure is known (25), we find that most of the key residues in PFOR that are involved in binding and activating TPP to generate the deprotonated ylide are conserved in OOR. These include β subunit residues Cys^{130} and Asn^{143} (Cys^{840} and Asn^{996} in *D. africanus* PFOR), which interact with the pyrophosphate moiety of TPP. Conserved residues that interact with the Mg^{2+} ion include a $G^{109}DGX_{32}N$ motif ($G^{962}DGX_{32}N$ in PFOR). Another key conserved residue is Asp^{59} (Asp^{64} in PFOR), which interacts with the N1′ pyrimidine group of TPP and plays a key role in deprotonation of the C-2 of the thiazole ring to generate the active ylide. Conserved residue Asn^{996} in PFOR (Asn^{143}) forms a hydrogen bonding interaction with the thiazolium sulfur of TPP, and a large hydrophobic residue, Phe^{869} of PFOR (Ile^{159} in the β subunit of OOR), interacts with TPP to promote formation of a V-conformation between the pyrimidine and thiazolium ring, which is conserved in all TPP-dependent enzymes so far studied. Different residues can stabilize the V-conformation in TPP-dependent enzymes; Ile is also found in this position in pyruvate decarboxylase (44), Met and Leu are found in pyruvate oxidase and transketolase, and other OFOR enzymes have His and Tyr.

Of the 2-oxoacid substrates we tested, oxalate was oxidized most quickly. Furthermore, the low K_m for oxalate ($\sim$60 μM) and the fact that the enzyme is induced in the presence of oxalate are consistent with oxalate being the physiological substrate for the enzyme. Although OOR can oxidize glyoxylate, the enzyme is not induced in cells grown on glyoxylate (14). Thus, we think it unlikely that OOR would be involved in glyoxylate metabolism in *M. thermoacetica*. OOR contains conserved residues that interact with the carboxyl and carbonyl groups of pyruvate in PFOR but contains substitutions that we propose are important for binding the carboxyl group of oxalate that replaces the acetyl group of pyruvate.

Several residues involved in pyruvate binding in PFOR are conserved in OOR, including Arg^{109} (Arg^{114} in PFOR, which binds the carboxyl group of pyruvate) and Asn^{143} (Asn^{996} in PFOR forms hydrogen bonds to the carbonyl group of pyruvate). Substitution of the Arg in *Sulfolobus tokodaii* that corresponds to Arg^{114} abolished activity (45). As expected, Ile^{123} and Ile^{843}, which interact with the methyl group of PFOR, are not conserved in OOR. Thr^{31} in PFOR is a highly conserved residue among the OFORs and is part of a YPITP motif that is important for catalysis. Substitutions of the end residues of this motif in an *Aeropyrum pernix* OFOR destroy activity, and separate mutations of the three middle residues have varying effects that are in general larger for k_{cat} than for K_m, which suggests that the motif is important during reaction turnover (26). However, Thr^{31} is replaced with Arg^{31} in the OOR. Inclusion of a second Arg in the active site may help to stabilize the additional negative charge on oxalate. Because Arg in this position is found in only those few sequences in the NCBI protein data base that have high identity to that of OOR, we propose that a YPIRP motif replaces the usual conserved YPITP motif to promote interactions that may be characteristic of OORs.

Decarboxylation and Electron Transfer—In analogy to the mechanism of PFOR (24), a general base would be expected to stabilize the negative charge on the oxalyl-TPP intermediate in step 3, followed by decarboxylation of the oxalyl-TPP adduct in step 4 to yield a reactive anionic carboxy-TPP intermediate that, in step 5, would release two electrons into the internal electron transfer pathway consisting of three $[Fe_4S_4]^{2+/1+}$ clusters. OOR contains sufficient iron to accommodate these three clusters. In addition, all 12 Cys residues that bind the three clusters of PFOR are conserved in the sequence of OOR. Furthermore, EPR and UV-visible experiments clearly showed that OOR contains three $[Fe_4S_4]^{2+/1+}$ and that oxalate can reduce all of these clusters. Because oxalate is a two-electron donor, full reduction of all of the clusters would require 2 mol of oxalate.

Because $[Fe_4S_4]$ clusters accept one electron at a time, there is likely to be a transient intermediate in which one of the clusters is reduced by the anionic carboxy-TPP anion to generate a carboxy-TPP radical (not shown); transient kinetic experiments are under way to test this hypothesis.

In this step of the PFOR reaction, binding of CoA accelerates the electron transfer reaction by 10^5-fold. However, OOR is a unique member of this family in having no requirement for CoA; therefore, step 6 would involve a second decarboxylation to regenerate the active ylide for the next round of catalysis. Although it seems less likely, it is possible that this carboxy-TPP adduct undergoes hydrolysis to release bicarbonate instead of CO_2. One of the proposed roles of CoA in PFOR and other OFORs is to generate a highly reducing anionic intermediate that could transfer electrons to the clusters (24, 46), and the same role has been proposed for phosphate in *Lactobacillus plantarum* pyruvate oxidase, which forms acetyl-phosphate and CO_2 from pyruvate (47). Perhaps the negative charge on the OOR carboxy-TPP adduct is sufficiently reducing to make CoA unnecessary.

In the final steps of the reaction, the two-electron-reduced state of OOR transfers its reducing equivalents from the internal electron transfer wire of $[Fe_4S_4]$ clusters to an external electron acceptor. Like PFOR, OOR can use a wide range of acceptors and is unable to transfer electrons to pyridine nucleotides. Ferredoxin is one of these and is a likely physiological electron acceptor that could carry electrons to enzymes of the Wood-Ljungdahl pathway. The rates were similar among all electron acceptors that were found to work. This suggests that the rate of catalysis is limited by some step other than electron transfer from the enzyme to the acceptor. Interestingly, like PFOR, OOR can transfer electrons directly to CODH to generate CO. This could be a physiologically relevant reaction *in vivo* because electrons from oxalate are used in the synthesis of acetyl-CoA (3) and because *M. thermoacetica* can be cultured on oxalate even in CO_2-free medium (14).

We propose that under CO_2-limiting conditions, CO_2 as well as electrons could be channeled directly from OOR to CODH. This would be an extremely interesting three-component channeling machine because it is clear that CO is channeled from CODH to ACS (41, 48).

REFERENCES

1. Fröstl, J. M., Seifritz, C., and Drake, H. L. (1996) *J. Bacteriol.* **178,** 4597–4603
2. Arendsen, A. F., Soliman, M. Q., and Ragsdale, S. W. (1999) *J. Bacteriol.* **181,** 1489–1495
3. Seifritz, C., Fröstl, J. M., Drake, H. L., and Daniel, S. L. (2002) *Arch. Microbiol.* **178,** 457–464
4. Strobel, B. W. (2001) *Geoderma* **99,** 169–198
5. Anantharam, V., Allison, M. J., and Maloney, P. C. (1989) *J. Biol. Chem.* **264,** 7244–7250
6. Baetz, A. L., and Allison, M. J. (1989) *J. Bacteriol.* **171,** 2605–2608
7. Allison, M. J., Dawson, K. A., Mayberry, W. R., and Foss, J. G. (1985) *Arch. Microbiol.* **141,** 1–7
8. Quayle, J. R., and Keech, D. B. (1959) *Biochem. J.* **72,** 623–630
9. Quayle, J. R. (1963) *Biochem. J.* **89,** 492–503
10. Costelloe, S. J., Ward, J. M., and Dalby, P. A. (2008) *J. Mol. Evol.* **66,** 36–49
11. Tanner, A., Bowater, L., Fairhurst, S. A., and Bornemann, S. (2001) *J. Biol. Chem.* **276,** 43627–43634
12. Woo, E. J., Dunwell, J. M., Goodenough, P. W., Marvier, A. C., and Pickersgill, R. W. (2000) *Nat. Struct. Biol.* **7,** 1036–1040
13. Seifritz, C., Fröstl, J. M., Drake, H. L., and Daniel, S. L. (1999) *FEMS Microbiol. Lett.* **170,** 399–405
14. Daniel, S. L., and Drake, H. L. (1993) *Appl. Environ. Microbiol.* **59,** 3062–3069
15. Daniel, S. L., Pilsl, C., and Drake, H. L. (2004) *FEMS Microbiol. Lett.* **231,** 39–43
16. Lundie, L. L., Jr., and Drake, H. L. (1984) *J. Bacteriol.* **159,** 700–703
17. Barent, R. L., and Elthon, T. E. (1992) *Plant Mol. Biol. Rep.* **10,** 338–344
18. Antonini, E., and Brunori, M. (1971) *Hemoglobin and Myoglobin in Their Reactions with Ligands*, p. 19, North-Holland Publishing Co., Amsterdam
19. Elliott, J. I., and Brewer, J. M. (1978) *Arch. Biochem. Biophys.* **190,** 351–357
20. Penttinen, H. K. (1979) *Methods Enzymol.* **62,** 58–59
21. Pierce, E., Xie, G., Barabote, R. D., Saunders, E., Han, C. S., Detter, J. C., Richardson, P., Brettin, T. S., Das, A., Ljungdahl, L. G., and Ragsdale, S. W. (2008) *Environ. Microbiol.* **10,** 2550–2573
22. Abe, K., Ruan, Z. S., and Maloney, P. C. (1996) *J. Biol. Chem.* **271,** 6789–6793
23. Zhang, Q., Iwasaki, T., Wakagi, T., and Oshima, T. (1996) *J. Biochem.* **120,** 587–599
24. Furdui, C., and Ragsdale, S. W. (2002) *Biochemistry* **41,** 9921–9937
25. Chabrière, E., Charon, M. H., Volbeda, A., Pieulle, L., Hatchikian, E. C., and Fontecilla-Camps, J. C. (1999) *Nat. Struct. Biol.* **6,** 182–190
26. Fukuda, E., Kino, H., Matsuzawa, H., and Wakagi, T. (2001) *Eur. J. Biochem.* **268,** 5639–5646
27. Kerscher, L., and Oesterhelt, D. (1981) *Eur. J. Biochem.* **116,** 587–594
28. Ma, K., Hutchins, A., Sung, S. J., and Adams, M. W. (1997) *Proc. Natl. Acad. Sci. U. S. A.* **94,** 9608–9613
29. Meinecke, B., Bertram, J., and Gottschalk, G. (1989) *Arch. Microbiol.* **152,** 244–250
30. Park, Y. J., Yoo, C. B., Choi, S. Y., and Lee, H. B. (2006) *J. Biochem. Mol. Biol.* **39,** 46–54
31. Nishizawa, Y., Yabuki, T., Fukuda, E., and Wakagi, T. (2005) *FEBS Lett.* **579,** 2319–2322
32. Yamamoto, M., Arai, H., Ishii, M., and Igarashi, Y. (2003) *Biochem. Biophys. Res. Commun.* **312,** 1297–1302
33. Dörner, E., and Boll, M. (2002) *J. Bacteriol.* **184,** 3975–3983
34. Weast, R. C., and Astle, M. J. (eds) (1981) *CRC Handbook of Chemistry and Physics*, p. D-166, CRC Press, Inc., Boca Raton, FL
35. Pieulle, L., Guigliarelli, B., Asso, M., Dole, F., Bernadac, A., and Hatchikian, E. C. (1995) *Biochim. Biophys. Acta* **1250,** 49–59
36. Orme-Johnson, W. H., and Beinert, H. (1969) *Biochem. Biophys. Res. Commun.* **36,** 337–344
37. Mathews, R., Charlton, S., Sands, R. H., and Palmer, G. (1974) *J. Biol. Chem.* **249,** 4326–4328
38. Cammack, R., Kerscher, L., and Oesterhelt, D. (1980) *FEBS Lett.* **118,** 271–273
39. Cornick, N. A., and Allison, M. J. (1996) *Appl. Environ. Microbiol.* **62,** 3011–3013
40. Cornick, N. A., Yan, B., Bank, S., and Allison, M. J. (1996) *Can. J. Microbiol.* **42,** 1219–1224
41. Doukov, T. I., Blasiak, L. C., Seravalli, J., Ragsdale, S. W., and Drennan, C. L. (2008) *Biochemistry* **47,** 3474–3483
42. Menon, S., and Ragsdale, S. W. (1997) *Biochemistry* **36,** 8484–8494
43. Ragsdale, S. W. (2003) *Chem. Rev.* **103,** 2333–2346
44. Guo, F., Zhang, D., Kahyaoglu, A., Farid, R. S., and Jordan, F. (1998) *Biochemistry* **37,** 13379–13391
45. Fukuda, E., and Wakagi, T. (2002) *Biochim. Biophys. Acta* **1597,** 74–80
46. Astashkin, A. V., Seravalli, J., Mansoorabadi, S. O., Reed, G. H., and Ragsdale, S. W. (2006) *J. Am. Chem. Soc.* **128,** 3888–3889
47. Tittmann, K., Wille, G., Golbik, R., Weidner, A., Ghisla, S., and Hübner, G. (2005) *Biochemistry* **44,** 13291–13303
48. Seravalli, J., and Ragsdale, S. W. (2000) *Biochemistry* **39,** 1274–1277

SUPPLEMENTAL INFORMATION FOR

IDENTIFICATION AND CHARACTERIZATION OF OXALATE OXIDOREDUCTASE, A NOVEL THIAMINE PYROPHOSPHATE-DEPENDENT 2-OXOACID OXIDOREDUCTASE THAT ENABLES ANAEROBIC GROWTH ON OXALATE*

Elizabeth Pierce[1], Donald F. Becker[2] and Stephen W Ragsdale[1]

[1]Department of Biological Chemistry, University of Michigan, Ann Arbor, MI 48109-0606 and
[2]Department of Biochemistry, University of Nebraska-Lincoln, Lincoln, NE 68588-0664

Running head: Oxalate Oxidoreductase

Address correspondence to: Stephen W Ragsdale, Department of Biological Chemistry, University of Michigan, University of Michigan Medical School, 5301 MSRB III, 1150 W. Medical Center Drive, Ann Arbor, MI 48109-0606. Phone: (734) 615-4621; Fax: (734) 763-4581; email: sragsdal@umich.edu

Sequence analysis of OOR. 2-oxoacid:ferredoxin oxidoreductases are made up of a minimum of three conserved domains, alpha, beta and gamma, with an additional delta domain in most OFORs. The genomic arrangement and fusion of these domains varies, with some proteins consisting of two subunits (αγ-fusion and β, called αβ type), some having separate α, β, γ and δ subunits and some (like many bacterial PFORs, including the *M. thermoacetica* PFOR) containing all four domains fused. The residues involved in binding TPP and one $[Fe_4S_4]^{2+/1+}$ cluster are in the beta subunit (1). Enzymes that include the delta subunit have two additional $[Fe_4S_4]^{2+/1+}$ clusters that are involved in electron transfer from the TPP active site to ferredoxin (2). αβ type OFORs that lack delta subunits have only one $[Fe_4S_4]^{2+/1+}$ cluster per αβ. The OOR protein is made up of separate α and β subunits and a third subunit that is a fusion of γ and δ domains (Figure 2).

We performed separate clustal W alignments of the sequences of the three OOR subunits with those of corresponding subunits of biochemically characterized pyruvate, 2-oxoisovalerate, 2-oxoglutarate, indolepyruvate and broad specificity oxidoreductases (see caption to Figure 3). The chosen sequences included the *D. africanus* PFOR, which has been crystallized in complex with pyruvate (3), allowing us to determine whether or not oxoacid binding residues are conserved in OOR. In the beta subunit, residues Gly109, Asp110, Gly111 and Cys130 (Gly962, Asp963, Gly964 and Cys840 are the corresponding residues in the *D. africanus* PFOR), which coordinate TPP and the adjacent Mg^{2+} ion, are present in OOR, along with the four cysteines (Cys residues 24, 27, 52 and 225 in the beta subunit) that ligate the $[Fe_4S_4]$ cluster that is nearest TPP. The eight cysteine residues that bind the other two $[Fe_4S_4]$ clusters are conserved in the OOR delta subunit (Cys residues 261, 264, 267 and 300 ligate one cluster and 271, 290, 293 and 296 coordinate the other cluster).

Table S1. **Mass spectrometric identification of oxalate oxidoreductase**

Spot	NCBI accession number	JGI locus tag	Percent sequence coverage	Number of peptides identified by LC-MS/MS
1	YP_430442	Moth_1593	58	26
2	YP_430441	Moth_1592	80	40
3	YP_429140	Moth_0262	29	10
4	YP_430440	Moth_1591	48	18
5	YP_429140	Moth_0262	50	17

Fig. S1. **Native PAGE of purified OOR, SDS PAGE of *M. thermoacetica* cell extracts.** Lanes 1-3, SDS-PAGE. Lane 1: molecular mass marker; Lane 2: total cell protein from *M. thermoacetica* grown on 28 mM oxalate and 50 mM glucose; Lane 3: total cell protein from *M. thermoacetica* grown on 50 mM glucose. Lanes 4-6, native PAGE. Lane 4: molecular mass marker; Lane 5: 10 µg *M. thermoacetica* PFOR; Lane 6: 10 µg oxalate oxidoreductase.

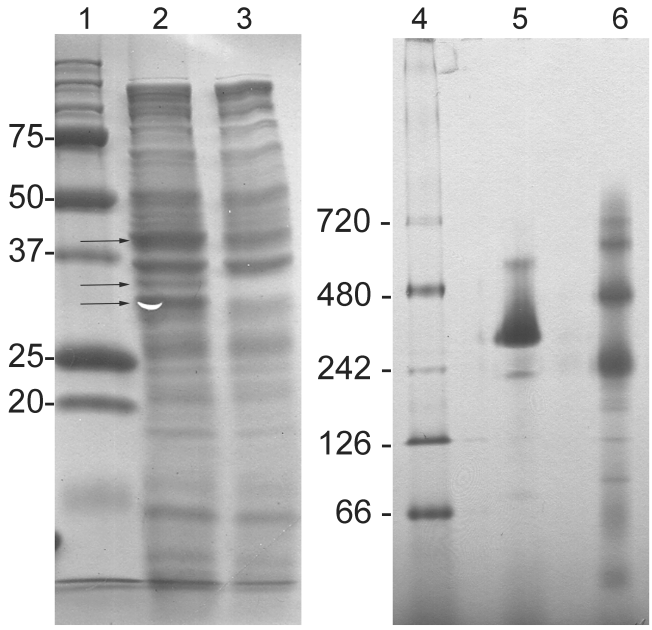

Fig. S2. **Two dimensional electrophoresis of oxalate oxidoreductase.** Molecular mass markers are visible at the left side of each gel. Cells were grown on CO_2 and *A*, oxalate; *B*, glucose and oxalate; *C,* glucose. Arrows point to the spots identified by mass spectrometry. The best match from the most predominant protein in each sample is listed in Table S1. Spots *1* and *2* were identified as the fusion of gamma and delta subunits and the alpha subunit of oxalate oxidoreductase. Two spots in *A* and *B* that are not well resolved (marked as *3* and *4*) are in the same position as a protein spot in *C* (marked as *5*). Spots *3* and *5* were identified as glyceraldehyde-3-phosphate dehydrogenase. Spot *4* was identified as the beta subunit of OOR. No peptides from this protein were identified in spot *5* from the gel from glucose-grown cells.

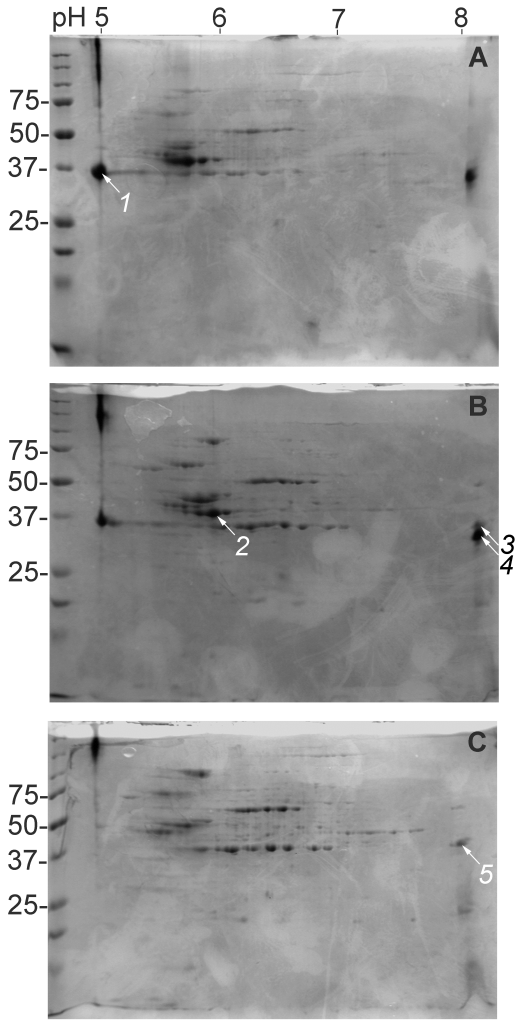

Fig. S3. **Gene cluster containing genes encoding OOR**

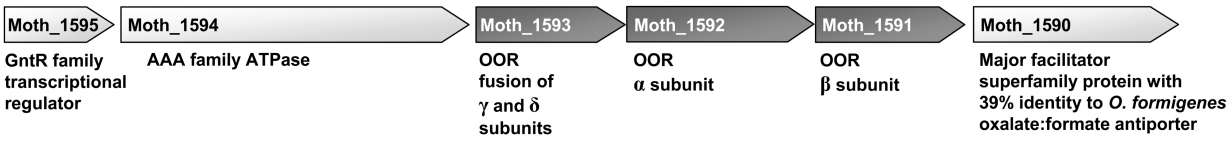

Fig. S4. **Size exclusion chromatography of purified OOR and PFOR.** *A*, elution of OOR (solid line) and pyruvate:ferredoxin oxidoreductase (dashed line) from the column. Elution was monitored by absorbance at 280 nm. *B*, standard curve used to calculate approximate molecular weights of OOR and PFOR. Ve/Vo is the ratio of the elution volume of each protein standard to the void volume of the column, determined using blue dextran.

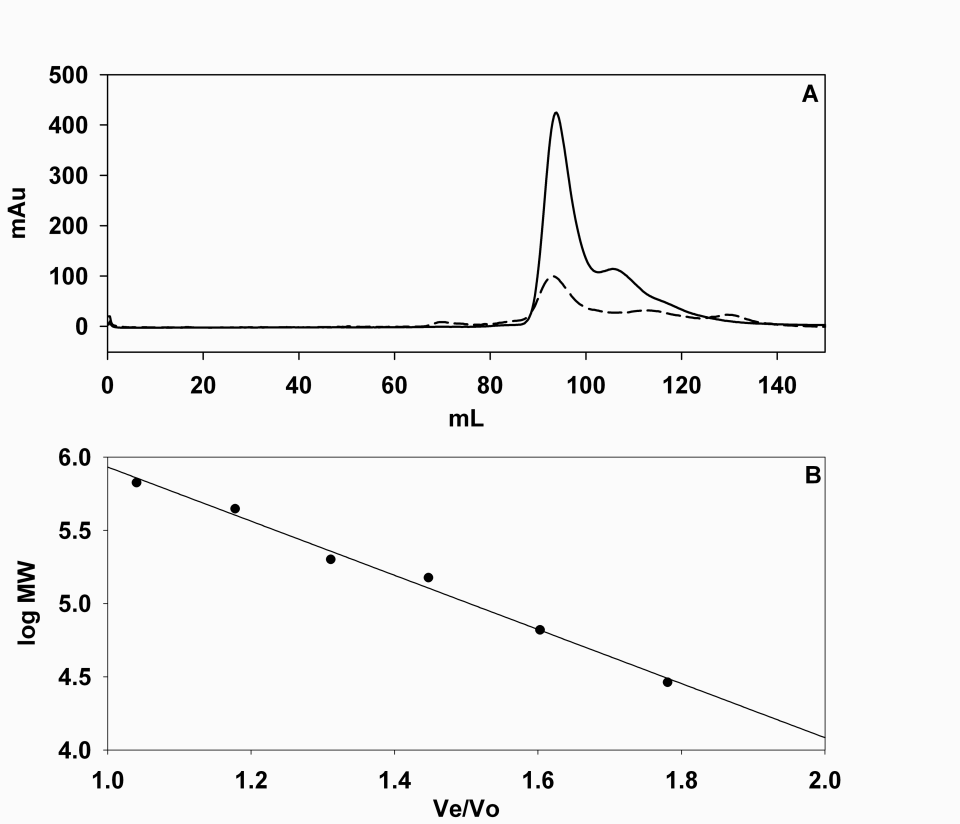

Fig. S5. **Alignment of 2-oxoacid:ferredoxin oxidoreductase sequences.** Alpha subunit sequences of pyruvate (por), 2-oxoisovalerate (vor), 2-oxoglutarate (kor) and indolepyruvate (ior) ferredoxin oxidoreductases, broad specificity 2-oxoacid:ferredoxin oxidoreductases (u) and four putative 2-oxoacid oxidoreductases from *M. thermoacetica* were aligned with the oxalate oxidoreductase alpha subunit (oor) using clustal W. The conserved YPITP substrate binding motif and the positions of two other residues that bind pyruvate in the *D. africanus* por crystal structure are highlighted. Species and NCBI sequence accession numbers are Moth: *M. thermoacetica* YP_430441 (oor), YP_428946 (por), YP_429255 (Moth_0378), YP_430765 (Moth_1922), YP_428916 (Moth_0033) and YP_430825 (Moth_1984); Mt: *Methanobacterium thermoautotrophicum* delta H (4) NP_276849 (por), O26800 (vor), NP_276168 (kor), and NP_276958 (ior); Pf: *Pyrococcus furiosus* (5,6) NP_578695 (por), NP_578698 (vor) and NP_578262 (ior); Hp: *Helicobacter pylori* (7) NP_207901 (por) and NP_207384 (kor); Eh: *Entamoeba histolytica* (8) AAB49653; Da: *Desulfovibrio africanus* (3) CAA70873; Ta: *Thermoanaerobacter tengcongensis* NP_622125; Am: *Alkaliphilus metalliredigens* YP_001322386; Ht: *Hydrogenobacter thermophilus* (9) BAA95605 (por), BAI69553 (kor1) and BAI69551 (kor2); Hs: *Halobacterium salinarum* (10) YP_001689139 (u) and NP_279533 (kor); Ta: *Thauera aromatica* (11) CAD27440; Ap: *Aeropyrum pernix* (12) NP_148403 (u1) and NP_147967 (u2); St: *Sulfolobus tokodaii* (13) NP_378302.

```
Moth_oor   20 ADVDVICSYPIRPYTGIMSELARMV 44     93  SPISGERLPVQMAIADRTLD-PPGDFGEEHTDAECCRDQG- 131
Mt_por     19 AKPKVIPVYPITPQTSISEYLAKFV 43     92  YAAAGLRNPIVMANANRALS-APLSIWNDQQDSIAERDSG- 130
Pf_por     20 AKPKVIAAFPITPSTLIPEKISEFV 44     93  FIAAGMRLPIVMAIGNRALS-APINIWNDWQDTISQRDTG- 131
Pf_vor     23 ARVQVVAAYPITPQTSIIEKIAEFI 47     93  HWAAGARLPIVMVDVNRAMA-PPWSVWDDQTDSLSQRDTG- 131
Moth_0378  20 ARVQVISAYPITPQSPIAEKLAEYV 44     93  GVASGCRVPIVMAVINRSLV-SPWSLWCDHQDSMAERDSG- 131
Moth_1922  18 ARAEVVAAYPITPQSTIVEKIAEYI 42     91  HYVSGCRVPLVMAVANRGLA-APWTIWADHQDAIACRDTG- 129
Hp_por     26 AQIDVIAAYPITPSTPIVQNYGSFK 50     99  YQASGMRLPIVLNLVNRALA-APLNIHGDHSDMYLSRDSG- 137
Eh_por     16 ALSDVSFIFPITPSSPMAENADVWS 40     94  IKIAGEHLPCVFHVTARALAGQALSIFGDHSDVMACRSTG- 132
Moth_por   18 AMSEVATIYPITPSSPMAEIADEWA 42     96  YKIAGELLPCVFHVAARALSTHALSIFGDHADVMAARQTG- 134
Da_por     20 AMSEVAAIYPITPSSTMGEEADDWA 44     98  YKISGELLPGVFHVTARAIAAHALSIFGDHQDIYAARQTG- 136
Tt_por     20 AFTEVAAIYPITPSSPMAELVDAWS 44     98  YKIAGELLPGVFHVSARAVATHALSIFGDHSDVMACRQTG- 136
Am_por     20 AFTDVAAIYPITPSSNMAENVDEWS 44     98  YKIAGELLPGVFHVSARALAGHALSIFGDHSDVMAVRQTG- 136
Ht_por     46 ASVDASVSYPITPQSEAAHLIGELW 70    118  PMWAGTRIPVQLVLMARGVN-APLSIQPDNLEVSFLLDTG- 156
Ht_kor1    36 ANVDIAIAYPITPQSEVMHLVGDLW 60    108  ASWPGHRIPAVLGVLTRVVN-APLSIQPDNVEIAYLLNCG- 146
Moth_0033  26 AGADIMYGYPITPQNEIMHYWTRM- 50     97  SMAEMMRLPTVVVVTQRGGPST-ATVIYSQQELNLTCFGG- 136
Mt_vor     14 AGCDCYFGYPITPASEILHEASRY- 38     95  SFLAGAELPAVIVDVMRAGP-GLGNIGPEQGDYNQIVKGGG 135
Moth_1984  18 AGCRVFAGYPITPATEIAENMARR- 42     90  GWAISSEIPLVIVNSQRVGPVVSGITGPGQGEFYLSRYLTH 129
Hp_kor     18 VGCRFFGGYPITPSSDIMHAMSVA- 42    100  GYSFMAEIPLVIADVMRSGPSTGMPTRVAQGDVNFLRHPI- 138
Mt_kor     21 AGCRFFAGYPITPSTEIAEEMALL- 45     93  GYAAMTETPLVIVNVQRGSPSSTGQPTASQSDMMQARWGS- 131
Hs_u      235 AGCRFISGYPMTPWTDAFTIMTQL- 259   307  GLAEMTETPLVLLEAQRAGPSTGMPTKPEQADLEHVLYTS- 345
Ht_kor2   213 AGCKFYAAYPITPATTVGNYIVED- 237   285  SYAGMTELPIVIVDVQRVGPATGMPTKHEQGDLYHAIYSG- 323
Ta_kor    216 GGVRFVAAYPITPGTEVLEWLAPN- 240   288  GLAVASETPITIVNVMRGGPSTGIPVKSEQSDLNIALYGM- 326
Hs_kor    214 AGCRFYAGYPITPATDVMEYLTGR- 238   286  GLVATSETPLVIANVMRSGPSTGMPTKQEQGDLNMMLKGG- 324
Ap_u1     258 GGVRYQAYYPITPASDESVLLEEFE 282   336  GWAGKNDVPMVITYYQRGGPSTGLPTRGSQSDLLFSLFAS- 374
St_u      245 GGVRFQSYYPITPASDESVYIEAHQ 269   328  GWAGMNEVPVVITYYIRGGPSTGLPTRTAQSDLIFPIFAG- 366
Ap_u2     255 GGLGVITYYPITPSSDEALYVEKHS 279   340  SLAVEAEIPVVVTLWMRAGPSTGMPTRTGQQDLLHSIFSG- 378
Mt_ior     30 SGVGVASTYPGTPSSEIGNVLSGIA 54     96  MSTAYTGVRAGMVVLTADDP-SMFSSQNEQDNRHYARLAC- 134
Pf_ior     32 GNIAVFAAYPGTPSSEVTDTMAAVA 56     98  MTVSYMGVNGGFIVMVADDP-SMWSSQNEQDTRAIGKFAN- 136
```

REFERENCES

1. Zhang, Q., Iwasaki, T., Wakagi, T., and Oshima, T. (1996) *Journal of Biochemistry* **120**, 587-599
2. Furdui, C., and Ragsdale, S. W. (2002) *Biochemistry* **41**, 9921-9937
3. Chabrière, E., Charon, M. H., Volbeda, A., Pieulle, L., Hatchikian, E. C., and Fontecilla−Camps, J. C. (1999) *Nature Structural Biology* **6**, 182-190
4. Tersteegen, A., Linder, D., Thauer, R. K., and Hedderich, R. (1997) *European Journal of Biochemistry* **244**, 862-868
5. Mai, X., and Adams, M. W. W. (1994) *Journal of Biological Chemistry* **269**(24), 16726-16732
6. Heider, J., Mai, X., and Adams, M. W. W. (1996) *Journal of Bacteriology* **178**(3), 780-787
7. Hughes, N. J., Clayton, C. L., Chalk, P. A., and Kelly, D. K. (1998) *Journal of Bacteriology* **180**(5), 1119-1128
8. Rosenthal, B., Mai, Z., Caplivski, D., Ghosh, S., de la Vega, H., Graf, T., and Samuelson, J. (1997) *Journal of Bacteriology* **179**(11), 3736-3745
9. Yun, N.-R., Arai, H., Ishii, M., and Igarashi, Y. (2001) *Biochemical and Biophysical Research Communications* **282**, 589-594
10. Kerscher, L., and Oesterhelt, D. (1981) *European Journal of Biochemistry* **116**, 587-594
11. Breese, K., Boll, M., Alt-Morbe, J., Schagger, H., and Fuchs, G. (1998) *European Journal of Biochemistry* **256**(1), 148-154
12. Nishizawa, Y., Yabuki, T., Fukuda, E., and Wakagi, T. (2005) *FEBS Letters* **579**(11), 2319-2322
13. Fukuda, E., and Wakagi, T. (2002) *Biochimica et Biophysica Acta - Protein Structure and Molecular Enzymology* **1597**, 74-80